ChemComm

COMMUNICATION

View Article Online
View Journal | View Issue

Cite this: *Chem. Commun.*, 2022, **58**, 11115

Received 18th July 2022,
Accepted 6th September 2022

DOI: 10.1039/d2cc04003d

rsc.li/chemcomm

Wet-spinning multi-component low-molecular-weight gelators to print synergistic soft materials†

Emma N. Drew,[a] Carmen C. Piras,[a] Juliette Fitremann[b] and David K. Smith*[a]

Two different low-molecular-weight gelators (LMWGs) have been 3D-printed as filaments by wet-spininng. When the two LMWGs are simultaneously wet-spun, the co-assembled hybrid gel filaments combine the individual properties of the two gelators (dynamic pH response and in-situ metal nanoparticle formation) in synergistic ways, creating gel objects with new properties.

Supramolecular hydrogels based on LMWGs that assemble *via* non-covalent interactions have *in vivo* applications such as drug delivery and tissue engineering.[1] They are responsive to stimuli, like solvent, pH, temperature *etc.*, and their properties can be influenced by self-assembly conditions.[2] The ability to shape and pattern such gels is increasingly valued, with a variety of techniques being explored.[3] 3D-printing has great potential, having been exploited with polymer-based gels.[4] However, 3D-printing remains relatively unexplored for LMWGs.

Adams and co-workers optimised parameters for extrusion printing a peptide gelator.[5] Others have printed peptide gels and in some cases, achieved 3D tissue culture.[6] Different types of supramolecular gel have also been printed.[7] Recently, Adams and co-workers 3D-printed LMWGs with layers of different concentrations.[8] The groups of Bai and Adams have printed layers of different peptide LMWGs.[9] Alternative to extrusion printing a pre-formed gel, a gel can rapidly form *in situ* after printing. Fitremann and co-workers pioneered LMWG wet-spinning.[10] An LMWG is dissolved at relatively high concentration in a good solvent; on injection into a poor solvent it assembles into a gel filament. This approach can also 3D-print LMWGs layer-by-layer onto a wet substrate. The stability of the printed objects can be enhanced by tuning hydrophobicity.[11]

Recently, we demonstrated that our thermally-responsive gelator DBS-CONHNH$_2$ based on 1,3:2,4-dibenzylidenesorbitol (DBS) was ideal for wet-spinning (Fig. 1), giving very stable 3D-printed objects.[12] Here, we extend this to a second LMWG – pH-responsive DBS-COOH (Fig. 1). We also determine whether the two gelators can be wet-spun in combination, with the goal of creating multi-component, multi-functional gel filaments. Multi-component gels are of considerable interest.[13] LMWGs may disrupt one another's assembly, self-sort, or co-assemble. Previously, multi-component gels of DBS-CONHNH$_2$ and DBS-COOH were formed, with the former assembled by slow cooling, and the latter *via* a slow pH drop.[14] The orthogonal approaches yielded self-sorted materials. Given printing multiple LMWGs is rare,[8] we were interested to know if two LMWGs could be simultaneously wet-spun giving gel filaments with synergistic behaviour.

The LMWGs were synthesised using our well-established methodology.[15] Gel filaments of DBS-CONHNH$_2$ were prepared by wet spinning as described previously.[12] We then explored wet-spinning DBS-COOH. A solution of DBS-COOH in DMSO

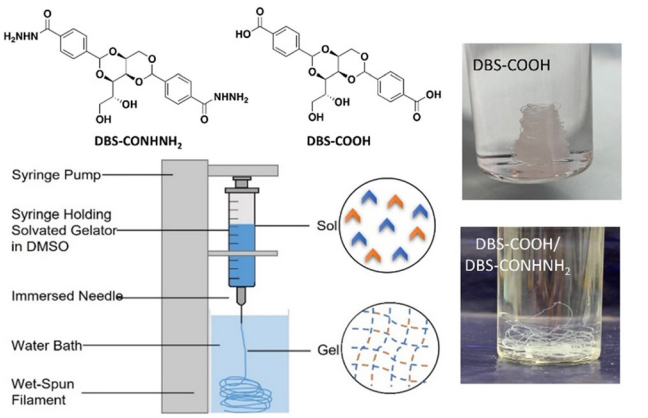

Fig. 1 Chemical structures of LMWGs DBS-CONHNH$_2$ and DBS-COOH, schematics of the experimental set-up for wet spinning and random co-assembly mode, and photos of gel filaments formed by DBS-COOH and DBS-COOH/DBS-CONHNH$_2$.

[a] *Department of Chemistry, University of York, Heslington, York, YO10 5DD, UK. E-mail: david.smith@york.ac.uk*
[b] *IMRCP, UMR 5623, CNRS, Université de Toulouse, 118 route de Narbonne, F-31062 Toulouse, France*

† Electronic supplementary information (ESI) available: Materials and methods, full characterisation and additional data. See DOI: https://doi.org/10.1039/d2cc04003d

formed gel filaments on injection into water (Fig. 1 and Fig. S1, ESI†). This was optimised (Fig. S2–S5, ESI†) in terms of loading (1.5–4.5% wt/vol‡), needle gauge (15–26G, 1.37–0.26 mm internal diameter, i.d.) and extrusion rate (3.4–27 μL min^{-1}). In general, at lower gelator loadings (1.5% wt/vol), with higher extrusion rates (>15 μL min^{-1}) uncontrolled gelation was observed in which a gel formed as an amorphous mass and was not spatially-constrained as a filament. Uncontrolled gelation resolved at higher loadings (≥3.0% wt/vol). At low extrusion rates (3.4 μL min^{-1}), needles with larger internal diameters (15G, 1.37 mm i.d. and 18G, 0.84 mm i.d.) sometimes gave issues with clogging. Our preferred conditions to extrude a continuous gel filament at all loadings were a flow rate of 3.4 or 6.7 μL min^{-1} through a 23G (0.34 mm i.d.) needle. Gel filament diameters ranged from 100–200 μm (Table S1, ESI†). Needle gauge had little effect, but concentration and flow rate had some impact, with higher concentrations and faster flow rates giving wider filaments. We estimated T_{gel} values by heating filaments in the absence of water. They had very good thermal stability with T_{gel} values of 88–98 °C, at loadings of 1.5–4.5% wt/vol (Table S2, ESI†). Unfortunately, the fragility of the filaments prevented rheology.

Scanning electron microscopy (SEM) showed filaments had a well-defined interior nanofibrillar network (Fig. 2(A) and Fig. S6, ESI†). Transmission electron microscopy (TEM) indicated nanofibers assembled with a relatively crystalline rigid, structure (Fig. 2(C) and Fig. S7, ESI†). This is different to DBS-COOH assembled *via* slow protonation, which has longer flexible gel fibres *ca.* 8–22 nm in diameter.[14a] We suggest the rapid assembly induced by wet-spinning leads to small crystal-like nanofibres rather than allowing for slow assembly of longer fibrillar objects.

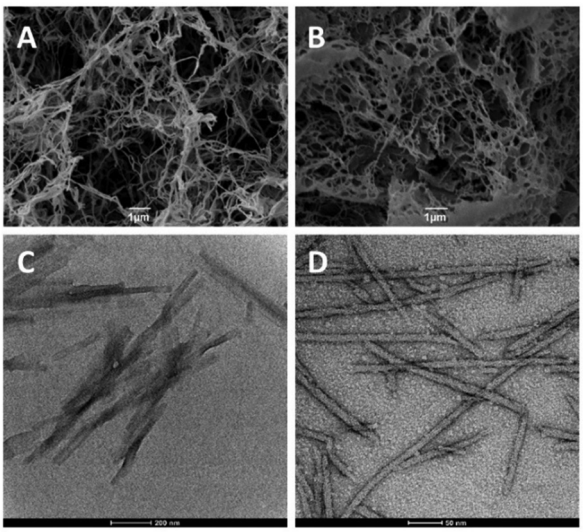

Fig. 2 SEM images of nanoscale structures that underpin the gel filaments formed by wet-spinning (A) DBS-COOH (4.5% wt/vol), scale bar = 1 μm and (B) DBS-$CONHNH_2$/DBS-COOH (4.5% wt/vol), scale bar = 1 μm. TEM images of gel filaments formed by wet-spinning (C) DBS-COOH (4.5% wt/vol), scale bar = 200 nm and (D) DBS-$CONHNH_2$/DBS-COOH (4.5% wt/vol), scale bar = 50 nm.

We quantified the LMWG in the filament by drying a sample, fully dissolving it in d_6-DMSO and adding an internal standard (CH_3CN). ^{1}H NMR indicated >99.5% of LMWG was incorporated at loadings of 1.5–3.0% wt/vol, and >95% at 4.5% wt/vol. The residual DMSO in the filaments was calculated as <1% by suspending filaments in D_2O with an internal standard. As in previous work,[12] washing filaments removed even more DMSO.

We then determined filament stability/dynamics (Table S3, ESI†). The LMWG (100 μL) was wet-spun into D_2O (6 ml), then transferred into an NMR tube with D_2O (0.7 ml). On standing, the DBS-COOH filaments formed at the lowest loading (1.5% wt/vol) slowly disassembled. After 1 day, 13% of the LMWG had become mobile, rising to 45% after 4 days (Fig. 3). Disassembly was less pronounced at higher loadings, with <5% of the LMWG becoming mobile. This suggests that at low DBS-COOH loading, ambient pH sufficiently deprotonates the LMWG to induce disassembly. Deprotonation will also occur at higher loadings, but presumably the nanofibers do not become sufficiently deprotonated for disassembly to trigger. In support of this, the pH of the water after wet-spinning fell (Fig. S9, ESI†), but at lower loadings the pH (as expected) fell less, giving a final pH (*ca.* 5.7) above the pK_a of DBS-COOH (5.4).[16] This demonstrates the inherent instability of DBS-COOH to ambient pH.[14] When gel filaments were exposed to NaOD/D_2O, DBS-COOH disassembly was complete (Fig. 3) in <5 min.

We then explored wet-spinning a combination of DBS-COOH and DBS-$CONHNH_2$ (Fig. S10–S15, ESI†). Equal mass loadings of each gelator were employed. At the lowest loading (0.75% wt/vol of each gelator, total loading 1.5% wt/vol), uncontrolled gelation was obtained at most flow rates, except the very slowest. As LMWG loading increased, filament formation increased, but at the highest loading (total load 6.0% wt/vol), clogs became increasingly common at low flow rates in larger needles. Our preferred conditions were a 23G needle at a flow rate of 3.4–10.2 μL min^{-1}, with total LMWG loading of 3.0% or 4.5% wt/vol. Filament diameters (130–230 μm) were somewhat dependent on loading; higher loadings giving wider filaments (Table S4, ESI†). T_{gel} values indicated very good thermal stability being 87–96 °C at LMWG loadings of 1.5–6.0% wt/vol (Table S5, ESI†).

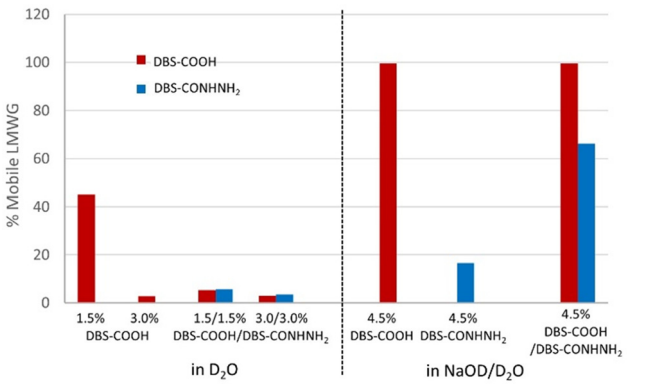

Fig. 3 Disassembly of gel filaments as monitored by ^{1}H NMR spectroscopy. (Left) % Mobile LMWG observed after 4 days standing in D_2O. (Right) % Mobile LMWG observed after 12 h standing in NaOD/D_2O.

SEM revealed a well-defined nanofibrillar interior network, similar to DBS-COOH alone, although there did appear to be some additional 'film-like' morphologies which could result from a drying artefact[17] (Fig. 2(B), and Fig. S16, ESI†). TEM, however, indicated different, very well-defined nanostructures (Fig. 2(D) and Fig. S17, ESI†). These appeared to be longer and more flexible than the DBS-COOH objects, and with darker edges, there was evidence they were nanotubular, with consistent diameters of 12.3 ± 2.5 nm. They were better defined than the nanofibers previously observed by TEM imaging of DBS-$CONHNH_2$-only filaments (with equivalent sample preparation).[12] The presence of a single well-defined nanoscale morphology suggests the LMWGs co-assemble into a new architecture when wet-spun together. This is different to self-sorted networks of these gels, formed using stepwise cooling/pH triggering,[14] which had 10–30 nm fibres. This indicates a different self-assembly pathway arises from rapid triggering achieved by the solvent switch mechanism used in wet spinning. We suggest this leads to random organisation of the gelators in co-assembled nanofibers. We were somewhat surprised by this as we had not previously observed co-assembly of these LMWGs, even though they have similar structures. It would be interesting in future to wet-spin LMWGs with very different structures to further understand this.

IR spectroscopy found that the N–H stretch shifted from a sharp band at 3295 cm^{-1} for filaments formed by DBS-$CONHNH_2$[12] to a broader band from 3180–3290 cm^{-1} for the two-component filament (Fig. S18 and S19, ESI†). The C=O stretch of DBS-COOH shifts slightly from 1689 cm^{-1} for wet-spun DBS-COOH to 1692 cm^{-1} for the two-component filaments (Fig. S20, ESI†). These changes suggest hydrogen bond interactions between the components, meaning the molecules intimately interact with each other when wet-spun together.

^1H NMR indicated >99% of each gelator assembled into filaments, with <1% residual DMSO present. On standing the filaments in D_2O, there was very little disassembly (<10%) over 4 days – even at the lowest total loading of 1.5% wt/vol (Fig. 3 and Table S6, ESI†). This is very different to DBS-COOH, where *ca.* 50% of LMWG became mobile. Wet-spinning in combination with DBS-$CONHNH_2$ stabilises the gel nanostructures at ambient pH. We suggest that once co-assembled with DBS-$CONHNH_2$, the ambient pH of water has less impact. In support of this, although pH initially falls on printing the two-component gel filaments, it then rises again suggesting an active role of DBS-$CONHNH_2$ in meditating pH (Fig. S21, ESI†) The stability of DBS-COOH in combination with DBS-$CONHNH_2$ in the filaments is different to self-sorted gels, in which, DBS-COOH disassembled even in the presence of DBS-$CONHNH_2$,[14] because they were sorted into their own nanostructures rather than in an intimate co-assembly. Wet-spinning is therefore promising for applying this two-component gel in tissue engineering,[18] as it should have the stability to survive in tissue growth medium.

We tested disruption of the two-component filaments with $NaOD/D_2O$. The DBS-COOH network was fully disrupted (Fig. 4 and Table S7, ESI†). In addition the DBS-$CONHNH_2$ network became >50% mobile (66% after 12 h). This suggests basic conditions fully deprotonate DBS-COOH, destabilising the nanostructures, breaking them down and releasing DBS-$CONHNH_2$. Not all of the DBS-$CONHNH_2$ becomes 'mobile', but its solubility is limited in water, which will limit the amount that can be observed. In contrast, DBS-$CONHNH_2$-only gel filaments are stable in basic conditions, with <20% of the gelator being mobilised (Fig. 3 and Table S8, ESI†). This supports the hypothesis that in the two-component wet-spun filaments, the gelators affect one another's behaviour because they are integrated into the same nanofibres. As such, DBS-COOH endows DBS-$CONHNH_2$ with base-responsiveness.

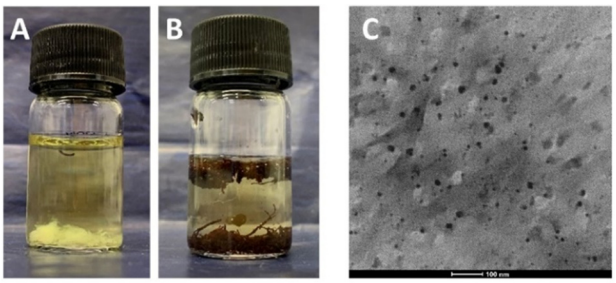

Fig. 4 Photographs of gel filaments based on (A) DBS-COOH and (B) DBS-$CONHNH_2$/DBS-COOH on exposure to aqueous $AuCl_3$ solutions. (C) TEM image of DBS-$CONHNH_2$/DBS-COOH gel after exposure to $AuCl_3$ and *in situ* formation of AuNPs (scale bar = 100 nm).

Finally, we tested the ability of these gel filaments to extract precious metals (*e.g.* Au(III)) from solution and form metal nanoparticles (*e.g.* AuNPs) *in situ* (Fig. 4). This is a distinctive behaviour of DBS-$CONHNH_2$-based gels not observed for other LMWGs and acts as a 'signature' of this molecule within a gel.[19] AuNP-loaded gels have applications as a result of their conductivity and biocompatibility (see below). On exposure of DBS-$CONHNH_2$/DBS-COOH gel filaments to $AuCl_3$ solution, an almost immediate colour change of filaments from white to purple was observed, consistent with AuNP formation (Fig. 4(B)). Conversely, for DBS-COOH-only gel filaments there was no colour change (Fig. 4(A)).

Gold uptake was quantified by UV-Vis spectroscopy (Table S9, ESI†). The two-component system incorporated increasing amounts of gold as the loading of DBS-$CONHNH_2$ increased. At total loadings of 1.5%, 3.0% and 4.5% wt/vol (0.75%, 1.5% and 2.25% wt/vol of DBS-$CONHNH_2$), Au uptake was 115, 140 and 164 μmol mL^{-1}, respectively. In our previous work on DBS-$CONHNH_2$-only gels, an LMWG loading of 1.5% wt/vol led to Au uptake of 127 μmol mL^{-1}.[12] This is comparable to the 140 μmol mL^{-1} observed for the multi-component system with equivalent DBS-$CONHNH_2$ loading, indicating DBS-$CONHNH_2$ retains its ability to reduce Au(III) to Au(0) in the presence of co-assembled DBS-COOH. Although DBS-COOH-only gels took up some Au(III), there was no evidence of reduction, and uptake was constant across all LMWG loadings, suggesting this is simple diffusion/partitioning, rather than specific interactions with the LMWG.

TEM images show AuNPs fairly uniformly dispersed within the two-component gel filaments (Fig. 4(C), and Fig. S23, ESI†).

There was some evidence of AuNPs in the DBS-COOH-only gel filaments (Fig. S22, ESI†) – but significantly fewer, and there were also significant areas of larger aggregates suggesting no control over metal uptake.

In conclusion, DBS-COOH, like DBS-$CONHNH_2$, can be wet-spun into gel filaments *via* DMSO/H_2O solvent-exchange. The DBS-COOH filaments can be dynamically disassembled by the addition of base, and at low loadings are prone to disassemble in water. On wet-spinning DBS-COOH in combination with DBS-$CONHNH_2$, a new co-assembled tubular nanostructure results. Importantly, the presence of DBS-$CONHNH_2$ stabilises the gel filaments in water and prevents DBS-COOH disassembly. However, the presence of DBS-COOH makes the system base-sensitive and enables base-triggered DBS-$CONHNH_2$ disassembly, which cannot be achieved for DBS-$CONHNH_2$-only gel filaments. The presence of DBS-$CONHNH_2$ allows the gel filaments to reduce precious metal salts to nanoparticles *in situ*, which cannot be achieved by DBS-COOH-only gels. Wet-spinning a combination of gelators therefore yields nanostructured gel filaments with a randomly co-assembled nanostructure, that could not previously be accessed. This harnesses the dynamic properties of DBS-COOH alongside the reducing ability of DBS-$CONHNH_2$ in a synergistic way to form stable but responsive filaments with incorporated AuNPs. Future work will test the biocompatibility of these filaments, and use them in layer-by-layer 3D-printing. Loading gels with AuNPs can enhance cell growth, and endow conductivity,[19] which could give such filaments impact in 3D scaffolds for electrical stimulus-responsive cells (*e.g.* stem cells, neurons, muscles).

The project was supervised by DKS who developed the concept. END performed experimental work and data interpretation. CCP provided training in wet-spinning. JF helped develop the experimental set-up in York. DKS helped with data analysis, and wrote the manuscript with input from all other authors.

We thank Karen Hodgkinson (Dept of Biology, Univ. York) for SEM and TEM imaging and Lamisse El-Qarra for image analysis. CCP thanks RSC (Mobility Grant, M19-9519) for funding.

Conflicts of interest

There are no conflicts to declare.

Notes and references

‡ A loading of 1.5% wt/vol means 15 mg of LMWG are dissolved in 1.0 ml DMSO. Given the density of DMSO is 1.10 mg mL^{-1}, this is equivalent to a loading of 1.36% wt/wt.

1 (*a*) X. Du, J. Zhou, J. Shi and B. Xu, *Chem. Rev.*, 2015, **115**, 13165–13307; (*b*) J. Hoque, N. Sangaj and S. Varghese, *Macromol. Biosci.*, 2019, **19**, e1800259.
2 (*a*) R. G. Weiss, *J. Am. Chem. Soc.*, 2014, **136**, 7519–7530; (*b*) E. R. Draper and D. J. Adams, *Chem*, 2017, **3**, 390–410; (*c*) D. B. Amabilino, D. K. Smith and J. W. Steed, *Chem. Soc. Rev.*, 2017, **46**, 2404–2420; (*d*) S. Panja and D. J. Adams, *Chem. Soc. Rev.*, 2021, **50**, 5165–5200.
3 (*a*) P. R. A. Chivers and D. K. Smith, *Nat. Rev. Mater.*, 2019, **4**, 463–478; (*b*) G. A. Primo and A. Mata, *Adv. Funct. Mater.*, 2021, **31**, 2009574.
4 (*a*) J. Li, C. Wu, P. K. Chu and M. Gelinksy, *Mater. Sci. Eng. Rep.*, 2020, **140**, 100543; (*b*) A. Kjar, B. McFarland, K. Mecham, N. Harward and Y. Huang, *Bioact. Mater.*, 2021, **6**, 460–471; (*c*) S. Bom, R. Ribeiro, H. M. Ribeiro, C. Santos and J. Marto, *Int. J. Pharm.*, 2022, **615**, 121506.
5 M. C. Nolan, A. M. Fuentes Caparrós, B. Dietrich, M. Barrow, E. R. Cross, M. Bleuel, S. M. King and D. J. Adams, *Soft Matter*, 2017, **13**, 8426–8432.
6 (*a*) Y. Xia, M. Qin, Y. Cao, Y. Li and W. Wang, *Sci. Rep.*, 2017, **7**, 9691; (*b*) B. Raphael, T. Khalil, V. L. Workman, A. Smith, C. P. Brown, C. Streuli, A. Saiaini and M. Domingos, *Mater. Lett.*, 2017, **190**, 103–106; (*c*) H. H. Susapto, D. Alhattab, S. Abdelrahman, Z. Khan, S. Alshehri, K. Kahin, R. Ge, M. Moretti, A.-H. Emwas and C. A. E. Hauser, *Nano Lett.*, 2021, **21**, 2719–2729; (*d*) S. Rauf, H. H. Susapto, K. Kahin, S. Alshehri, S. Abdelrahman, J. H. Lam, S. Asad, S. Jadhav, D. Sundaramurthi, X. Gao and C. A. E. Hauser, *J. Mater. Chem. B*, 2021, **9**, 1069–1081; (*e*) N. A. Sather, H. Sai, I. R. Sasselli, K. Sato, W. Ji, C. V. Synatschke, R. T. Zambrotta, J. F. Edelbrock, R. R. Kohlmeyer, J. O. Hardin, J. D. Berrigan, M. F. Durstock, P. Mirau and S. I. Stupp, *Small*, 2021, **17**, 2005743; (*f*) J. Yang, M. Chen, H. Lee, Z. Xu, Z. Zhou, S.-P. Feng and J. T. Kim, *ACS Appl. Mater. Interfaces*, 2021, **13**, 20573–20580.
7 (*a*) H. Yang, S. Zhang, K. Liu and Y. Fang, *RSC Adv.*, 2016, **6**, 109969; (*b*) K. Liu, S. Zang, R. Xue, J. Yang, L. Wang, J. Huang and Y. Yan, *ACS Appl. Mater. Interfaces*, 2018, **10**, 4530–4539; (*c*) A. Biswas, S. Malferran, D. M. Kalaskar and A. K. Das, *Chem. Commun.*, 2018, **54**, 1778–1781; (*d*) B. Dessane, R. Smirani, G. Bouguéon, T. Kauss, E. Ribot, R. Devillard, P. Barthélémy, A. Naveau and S. Crauste-Manciet, *Sci. Rep.*, 2020, **10**, 2850; (*e*) Z. Zhou, M. Samperi, L. Santu, G. Dizon, S. Aboarkaba, D. Límon, C. Tuck, L. Pérez-García, D. J. Irvine, D. B. Amabilino and R. Wildman, *Mater. Des.*, 2021, **206**, 109792; (*f*) G. Yang, R. Guan, H. Zhen, K. Ou, J. Fang, D. Li, Q. Fu and Y. Sun, *ACS Appl. Mater. Interfaces*, 2022, **14**, 10998–11005.
8 A. M. Fuentes-Caparrós, Z. Canales-Galarza, M. Barrow, B. Dietrich, J. Läuger, M. Nemeth, E. R. Draper and D. J. Adams, *Biomacromolecules*, 2021, **22**, 1625–1638.
9 (*a*) H. Jian, M. Wang, Q. Dong, J. Li, A. Wang, X. Li, P. Ren and S. Bai, *ACS Appl. Mater. Interfaces*, 2019, **11**, 46419–46426; (*b*) M. J. S. Hill and D. J. Adams, *Soft Matter*, 2022, **18**, 5960–5965.
10 (*a*) A. Chalard, P. Joseph, S. Souleille, B. Lonetti, N. Saffon-Merceron, I. Loubinoux, L. Vaysse, L. Malaquin and J. Fitremann, *Nanoscale*, 2019, **11**, 15043–15056; (*b*) A. Chalard, M. Mauduit, S. Souleille, P. Joseph, L. Malaquin and J. Fitremann, *Addit. Manuf.*, 2020, **33**, 101162; (*c*) D. Bordignon, B. Lonetti, C. Coudret, P. Roblin, P. Joseph, L. Malaquin, A. Chalard and J. Fitremann, *J. Colloid Interface Sci.*, 2021, **603**, 333–343.
11 F. Andriamiseza, D. Bordignon, B. Payré, L. Vaysse and J. Fitremann, *J. Colloid Interface Sci.*, 2022, **617**, 156–170.
12 C. C. Piras, A. G. Kay, P. G. Genever, J. Fitremann and D. K. Smith, *Chem. Sci.*, 2022, **13**, 1972–1981.
13 E. R. Draper and D. J. Adams, *Chem. Soc. Rev.*, 2018, **47**, 3395–3405.
14 (*a*) C. C. Piras and D. K. Smith, *Chem. – Eur. J.*, 2019, **25**, 11318–11326; (*b*) L. Schlichter, C. C. Piras and D. K. Smith, *Chem. Sci.*, 2021, **12**, 4162–4172; (*c*) H. S. Cooke, L. Schlichter, C. C. Piras and D. K. Smith, *Chem. Sci.*, 2021, **12**, 12156–12164.
15 (*a*) D. J. Cornwell, B. O. Okesola and D. K. Smith, *Soft Matter*, 2013, **9**, 8730–8736; (*b*) B. O. Okesola and D. K. Smith, *Chem. Commun.*, 2013, **49**, 11164–11166.
16 D. J. Cornwell, O. J. Daubney and D. K. Smith, *J. Am. Chem. Soc.*, 2015, **137**, 15486–15492.
17 D. J. Adams, *Gels*, 2018, **4**, 32.
18 B. O. Okesola, Y. Wu, B. Derkus, S. Gani, D. Wu, D. Knani, D. K. Smith, D. J. Adams and A. Mata, *Chem. Mater.*, 2019, **31**, 7883–7897.
19 B. O. Okesola, S. K. Suravaram, A. Parkin and D. K. Smith, *Angew. Chem., Int. Ed.*, 2016, **55**, 183–187.

